The Egyptian International Journal of Engineering Sciences and Technology

Vol. 29 (2020) 28–42

http://www.eijest.zu.edu.eg

ISSN:1687-1006

NUMERICAL ANALYIS OF AMMONIA/HYDROGEN FLAMES IN A SWIRL AND BLUFF-BODY STABILIZED BURNER

Mohamed Yehia*, Fawzy Abdel-Aziz and Hatem O. Haridy

Department of Mechanical Power, Faculty of Engineering, Cairo University, Giza, Egypt

ARTICLE INFO

Article history:
Received 09 December 2019
Received in revised form
01 March 2020
Accepted 03 March 2020
Available online 10 March 2020

Keywords:
CFD burner design,
premixed and partially premixed modelling,
ammonia-hydrogen mixtures,
flame stability

ABSTRACT

Ammonia (NH_3) is a possible and attractive substitute of hydrocarbon fuels in the path towards achieving clean energy goals. Key obstacles that require immediate attention are its relatively low reactivity and high NO_x emissions. A proper investigation of both issues call for an in depth consideration of the near burner flow aerodynamics. CFD has played a significant role in suggesting innovative burner designs to overcome particular problems under circumstances of single and two-phase reacting flows. This study is part of a broader investigation dealing with the development of a novel combustor for ammonia firing. Reynolds Averaged Navier Stokes (RANS) analysis of a swirl and bluff-body stabilized burner firing various mixtures of NH_3 and H_2 was performed. The effect of the burner configuration and H_2 content in the fuel mixture on the internal recirculation zone was examined. As the firing conditions imply non-diffusion flame, both premixed and partially premixed combustion modelling with various combustion models were used for the investigation. Three stoichiometric mixtures with pure ammonia, 25% H_2 and 50% H_2 blends were studied. In some cases, simulations suggested flash back into the 'fresh charge' tube preceding the chamber. While the flame for pure ammonia firing was longer, the introduction of hydrogen in the fuel mixture increased the reactivity, as typified by the higher temperature and product formation rate.

1. INTRODUCTION

The world is continuously and gradually restricting the burning of carbon-based fuels that are posing excessive damage to the environment and climate change. Implementation of renewable energy sources such as wind energy for grid power are beginning to show flaws that need attention [1]. Ammonia continues rising as an attractive candidate and complementary vital element in the complete setup of future clean energy diagram. The numerous advantages that are considered by energy decision makers include its well-established infra-structure with its historical background in the agricultural fertilizing and cooling fields for the past century with proven reliability, its high hydrogen content and straight forward cracking techniques required to produce back pure hydrogen indicating that it is the clean and safe hydrogen carrier that contains more hydrogen than hydrogen. Relatively easier and cheaper arrangements for storage through longer duration of time and transportation distances sought for and the safe handling justify its consideration as the main hydrogen enabler. The well-established means of synthesizing ammonia both from renewable (green) and well established conventional (brown) sources, its preferable properties including volume and mass energy densities, relatively mild pressure needed for liquification, higher autoignition temperature, are but some of the many points to

* Corresponding author. Tel.: 01003269999
E-mail address: myehia@cu.edu.eg.

justify its future prominence in the energy market,[2], [3].

Landmarks in the historical path of ammonia dates back to the 1916 establishment of the Haber-Boch process of manufacturing ammonia [4], better known as steam-reforming technique. The production and utilization of ammonia as a fertilizer is considered to be a main driver towards boosting the growth of food and thus the increase in global population from 1.6 billion inhabitants then to the present 6 billion inhabitants. The years of world war II experienced a challenge of unavailability of produced and transported fossil fuel derivatives required to maneuver armies around a vast battlefield gave way to running public transport busses in Belgium using ammonia as its fuel. On the 1960s, NASA produced a hypersonic ammonia LOX X-15 rocket motor achieving Mach number of 6.72.

On the other hand, hydrogen poses acute safety challenges especially with its wide flammability range, high reactivity, and relatively low ignition temperature.

The blending of ammonia with other fuels including hydrogen enhances its inherently low flame speed and reactivity and thus is always the first step towards obtaining a stable combustion with accepted overall characteristics and reduced emissions. Blending ammonia with hydrogen is possible as the later may be obtained by cracking an amount of the ammonia stream through the use of a heat exchange that raises its temperature to 657 K, [5]. When blended with other fuels including gasoline, diesel, ethanol, methanol, propane, butane, natural gas, etc. in internal combustion engine power generation, it results in a decrease of deleterious emissions occurring after combustion, [6]. Furthermore, increases in both the overall energy and exergy efficiencies are observed. The only precaution considered was to replace any brass or copper parts exposed to ammonia by alternative stainless-steel manufactured ones to avoid its corrosive effect.

A 1-dimensional numerical study on which the amount of hydrogen in a rich fuel ammonia/hydrogen mixture of a power input of 10 kW at an equivalence ratio of 1.2 with increases in 10% steps of the ammonia fraction indicated that the lowest levels of unburned NH_3 were calculated in the 60-40 ammonia/hydrogen volumetric ratio. This mixture gave the highest levels of NO emissions. Further analysis by [5] suggested that the burner design can affect the flame topology. Once the best combustion behavior for a certain application is recommended, the problem of NO may be resolved through the application of a percentage of the ammonia/hydrogen mixture post of the flame central recirculation zone. Another 1-D study by [7] examined the effect of adding varying amounts of ammonia burning with methane air mixtures. They noted that at a fuel rich conditions, ammonia has a self-inhibition effect on its own oxidation. Higher concentrations of ammonia give lower NOx emissions than lower concentrations when burning rich fuel mixtures. They concluded that the addition of ammonia on a stoichiometric methane air mixture resulted in lowering the burning velocity and increasing the NO concentration. For example, the addition of 4% of ammonia gave a NO concentration of 3500 ppm in the combustion products. Chemical Kinetic simulations confirmed those results. It was observed that the addition of ammonia almost did not affect the formation of CO.

The stabilization and emission characteristics of ammonia/air premixed flames in swirl combustors were investigated by [8]. They considered the orange chemiluminescence that is emanating from the superheated steam and NH_2 radicals as representation of the flame structure. Those chemiluminescence images suggested that the rich ammonia-air mixtures gave brighter and more compact flame than that produced by the stochiometric or lean mixtures. A much shorter flame with a blue color was produced when using a methane air mixture under similar conditions in the same burner. This difference in behavior is due to the ammonia lower laminar burning velocity. They extracted stability maps for different equivalence ratios and inlet mixture velocities at swirl number range from 0.73 to 1.27. The experiments showed that a stable flame region may be obtained in the range of equivalence ratios from 0.6 to 1.4 which is narrower than that which may be obtained for methane at similar conditions. It was observed that there is a lower mixture velocity limit below which the flame would blow off whatever was the equivalence used. Their analysis of emissions suggested that higher levels of NO in excessive of 4000 ppm are produced at a lean mixture that start reducing for rich mixture. A selective catalytic reduction was proposed to obtain a simultaneous reduction in both NO and unburned NH_3.

Oxygen-enriched combustion of ammonia as a conduit to overcoming its inherent drawbacks was investigated by[9]who performed a numerical study on effect of oxygen content in combustion air on the characteristics of ammonia combustion. The study involved the oxygen enrichment between 21% to 30%. It was deduced that increasing oxygen in the

reactants results in increasing both the laminar burning velocity and the adiabatic flame temperature, both of which improve the combustibility of ammonia as a fuel. For example, 30% oxygen gives an increase of 2.6 times the laminar burning velocity reached with atmospheric air. However, the higher formation of HNO leads to higher levels of NO emissions. Those are reduced at fuel rich mixtures as is the case with burning atmospheric air.

As the use of conventional fossil fuels as power source for vehicular field is considered the main source of polluting air in populated cities, [6], assessed the impact on performance resulting from blending several fuels with ammonia in operating a SIE-generator of a maximum power of 3.65 kW. They modified some parts in a commercial generator to stand the expected higher temperatures at the exhaust and they also removed copper and brass parts and substituted them by steel parts to resist the expected ammonia corrosive effects. The study involved experimental measurements and numerical analysis with the use of EES (Engineering Equation Solver). The effects of increasing the ammonia blend from 20% gradually to 80% on the power output, exergy destruction rate, energy and exergy efficiencies for the fuels under consideration were demonstrated. The fuels studies included hydrogen, gasoline, diesel, propane, butane, natural gas, ethanol and methanol. Generally, the change from an initial point of 80% conventional fuel to a final point of 80% ammonia resulted in a reduction in the power output and the exergy destruction rate. The overall energy and exergy efficiencies increased slightly. The exhaust temperature increased with the increase of percentage of ammonia blend. However, the drastic positive change is the reduction of deleterious emissions occurring after combustion. This will be a considerable difference to protect the environment.

The detailed chemical kinetics for H/N/O mechanisms and that for ammonia combustion have been modeled by [10], [11], [12]. As scaling up of ammonia combustion is expected to take place in applications such as spark ignition engines, those models were scrutinized in conditions mimicking those inside a cylinder of a four stroke engine with varying temperatures and pressures experimentally and numerically by [13] aiming at validating and reducing the original model for the formation and destruction of pollutants and intermediate compounds such as nitrous oxide (N_2O), amidogen radical (NH_2), imidogen (NH), OH, NO, HO_2, N_2H_2, NO_2, etc. as well as the major species including NH_3, O_2, N_2, H_2O. Several corrections for the rate constants were suggested by[14]. In order to allow economical application of those kinetic models into CFD applications, reduced mechanisms were proposed that would involve for example 80 elementary reactions involving 19 chemical species.

The present work supports experimental investigations such as [15] that aimed at studying the stability map and emission range for different mixtures of ammonia and hydrogen at various equivalence ratios through the firing in a novel burner. The stability of the flame was ensured through a combination of a radial introduction of the combustion air together with the presence of a bluff body. The aerodynamic flow pattern plays a significant role as a priori to an improved stability range under different conditions. The present study only concentrates at stoichiometric reactions of 1900 watts powered burner obtained from 3 different fuel mixtures; ammonia with 0, 25 and 50% hydrogen. In the beginning of the study, two close designs of bluff bodies were studied to demonstrate the effect of the aerodynamics on stability. Thus, after the selection of the better burner, the analysis included a wide range of modelling techniques.

The study presented here involved the utilization of ANSYS R19 as a solver to the fluid flow, with axi-symmetric RANS, premixed and partially premixed assumptions. The ability of the present modelling techniques to provide an analysis a hydrogen/ammonia/air flame is assessed.

2. NUMERICAL SETUP

2.1. Geometry and Meshing

In the present work, axi-symmetric, steady/transient and RANS simulations were performed using ANSYS/Fluent program to study the effect of different hydrogen enrichments on the flow field dynamics, main combustion characteristics and stability of H_2/NH_3/Air flame at stoichiometric condition. An innovative design of swirl-bluff body-stabilized burner with two different geometries is assessed using ANSYS/Design Modeler program. The premixed air-fuel mixture is burned in the combustor space that has 100mm diameter and 320mm height. Initially, air is introduced tangentially inside the premixing tube of 400mm length, while fuel mixture is issued from 12 holes of 2mm diameter. The difference between the two burners configuration is presented in the annulus thickness that lies between the premixing tube and the bluff-

body. This thickness is 3mm for configuration (a) and 1mm for configuration (b) as shown in figure 1.

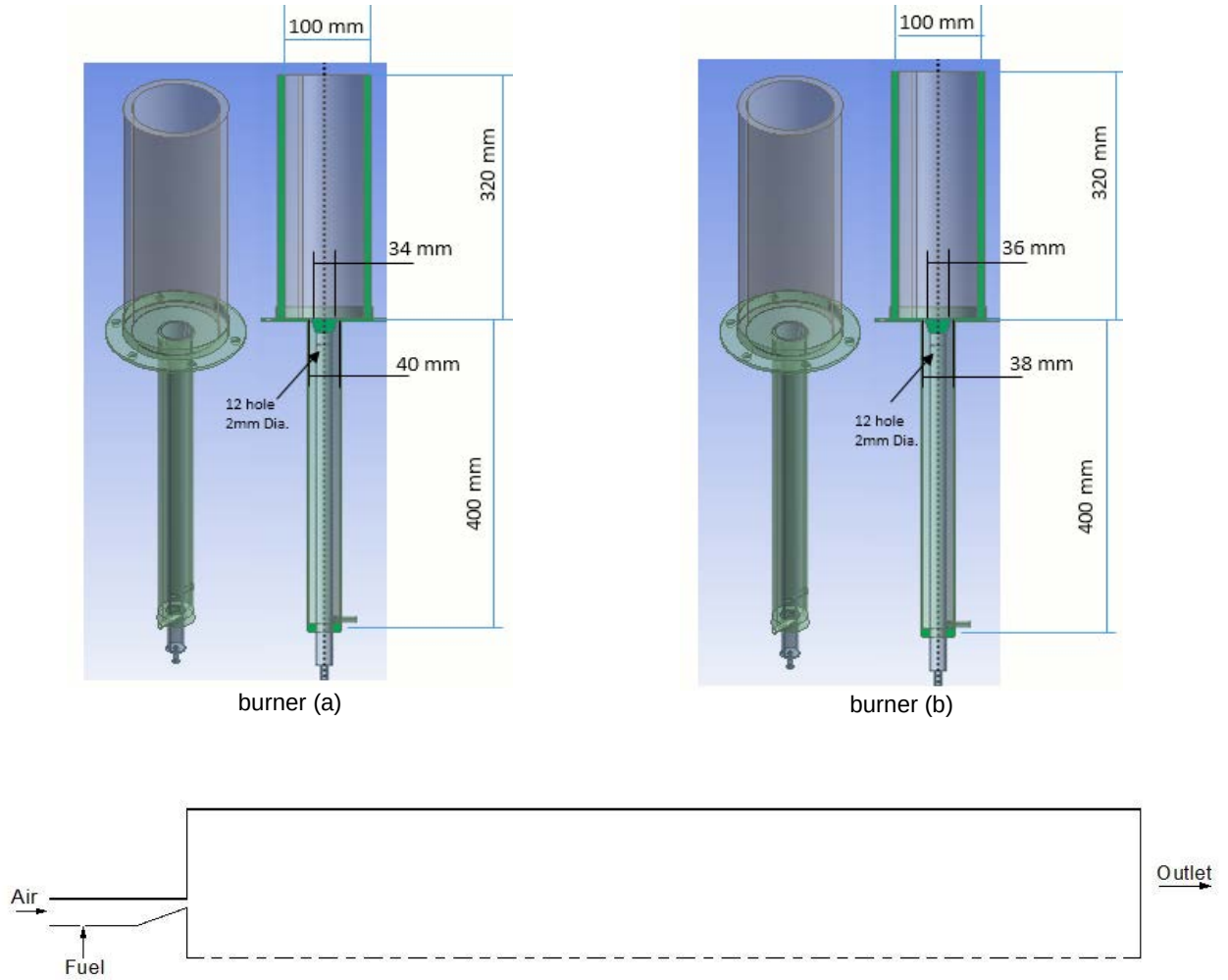

Fig. 1: Two burner configurations and the computational domain

The present mesh structure is based on Dynamic- locally refines the grid in the vicinity of flame front to intensify the solution accuracy with minimal computational time, see figure 2. After performing a grid independency test which is discussed later in results section, it is observed that the optimal meshing structure is constructed from three regions. Adaptive Grid Refinement (DAGR) strategy which The farthest domain which has a mesh size of 5 mm while the combustion chamber domain is of 2 mm mesh size and finally around the flame front, the mesh approaches 0.4 mm. The aspect ratio is of average 1.242, the skewness is 0.0073 and orthogonality of 0.955.

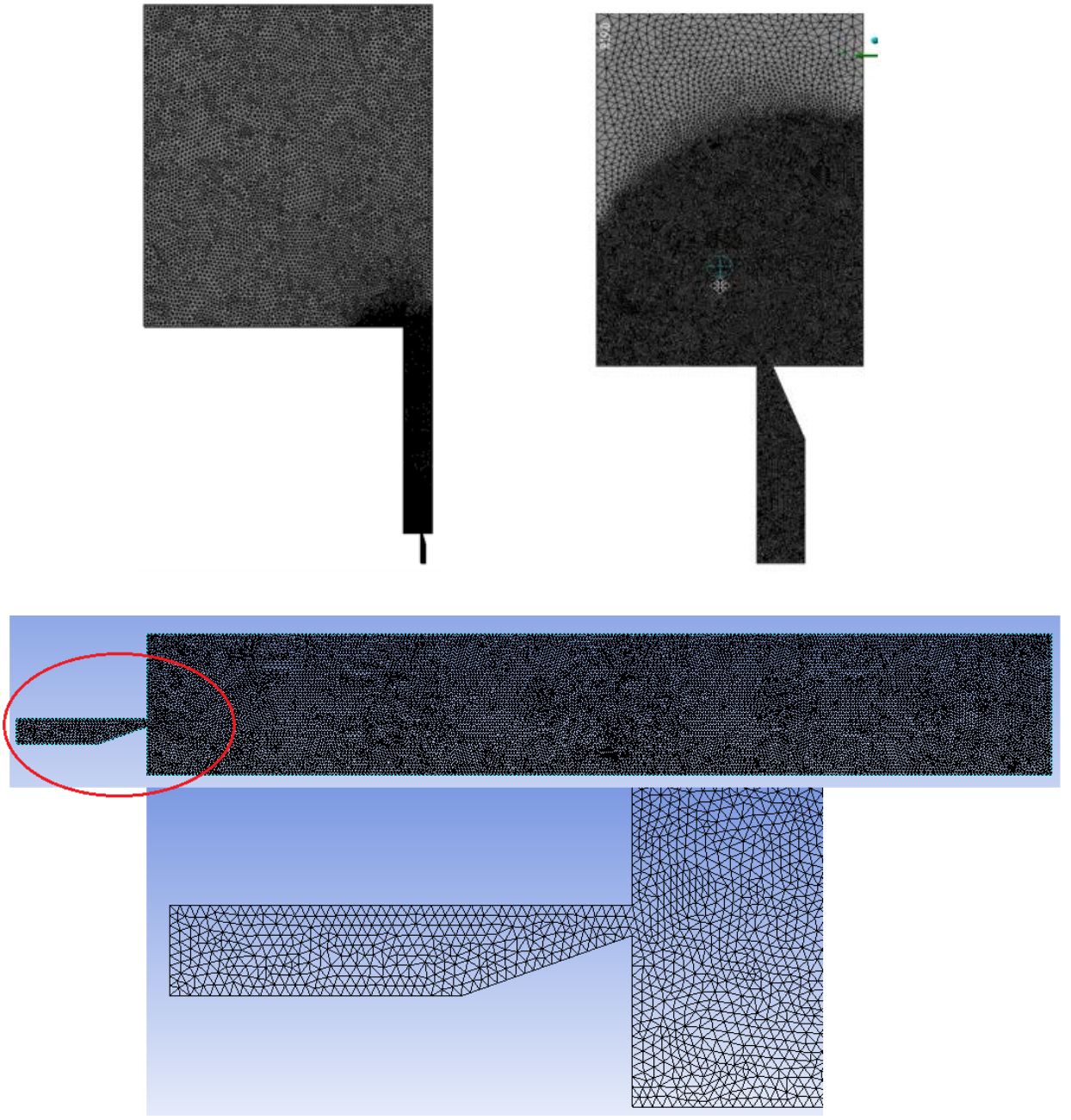

Fig. 2: Dynamic-Adaptive Grid Refinement (DAGR) through various regions of combustion domain

2.2 Mathematical Modelling

The numerical tool used in this study is the axi-symmetric cylindrical coordinate ANSYS R19 with its detailed formulation given in [16]. Only a brief is given in the following. While the equations used throughout this work are the cylindrical co-ordinates, (r and x) that may be obtained from for example [17], the equations given in the following demonstration are in the more general form. Transient formulations of the basic conservation equations of RANS are presented and solved as follows:

Mass conservation:

$$\frac{\partial \rho}{\partial t} + \frac{\partial}{\partial x_i}(\rho u_i) = 0 \quad (1)$$

Momentum conservation:

$$\frac{\partial}{\partial t}(\rho u_i) + \frac{\partial}{\partial x_j}(\rho u_i u_j) = -\frac{\partial p}{\partial x_i} + \frac{\partial}{\partial x_j}\left[\mu\left(\frac{\partial u_i}{\partial x_j} + \frac{\partial u_j}{\partial x_i} - \frac{2}{3}\delta_{ij}\frac{\partial u_l}{\partial x_l}\right)\right] + \frac{\partial}{\partial x_j}(-\rho\overline{u_i' u_j'}) \quad (2)$$

Species conservation:

$$\frac{\partial}{\partial t}(\rho Y_k) + \frac{\partial}{\partial x_i}(\rho u_i Y_k) = \frac{\partial}{\partial x_i}(\rho D \frac{\partial Y_k}{\partial x_i}) + \rho S_{Yk} \quad (3)$$

Energy conservation:

$$\frac{\partial}{\partial}(\rho E) + \frac{\partial}{\partial x_i}(\rho u_i E) + \frac{\partial}{\partial x_i}(u_i P) = \frac{\partial}{\partial x_i}(\lambda_{eff}\frac{\partial T}{\partial x_i} - \sum_{k=1}^{N} h_k \overrightarrow{J_k} + u_i \tau_{ij}) - \frac{\partial}{\partial x_j}(-\rho\overline{u_i' h_s'}) + q_c \quad (4)$$

where ρ is the density, u_i the velocity in i direction, E the total energy, h the enthalpy, *J* the diffusional flux, λ_{eff} the effective conductivity, Y_k the mass fraction of the k_{th} species, D the mass diffusivity and S_{Yk} the source term of the k_{th} species.

The source term qc in equation (4) is evaluated as follows:

$$q_c = \rho S_{Y_i} \Delta H \quad (5)$$

where ΔH is the heating value of fuel.

2.2.1 Turbulence models
Reynolds Stress Model (RSM)

Reynolds Stress Model (RSM) is adopted here to predict the turbulence characteristics in the flow. RSM does not apply the isotropic eddy-viscosity approximation as classical k-ε model do, but it basically solves the differential transport equations of Reynold's stress tensor. This transport equation of Reynolds stress does not have only convective and diffusion terms for the stress but it has production, buoyancy, pressure strain and dissipation terms to account for the effects of streamline curvature, rotation, and buoyancy of turbulent flows. Though this requires relatively longer computational time than the traditional k-ε model, but as the theme of the present study is to understand the impact of aerodynamic details on the stabilization of different gas mixtures of hydrogen ammonia blends, the determination of formulation and configuration of the internal recirculation zone is considered to be of key importance. RSM is considered to be of better performance on that aspect, [17] The transport equations of the Reynolds stresses term can be expressed as follows [18]:

$$\underbrace{\frac{\partial}{\partial t}(\rho\overline{u'_\iota u'_\jmath})}_{(local\ time\ derivative)} + \underbrace{\frac{\partial}{\partial x_k}(\rho x_k \overline{u'_\iota u'_\jmath})}_{(C_{ij}=\ convection)} = \underbrace{-\frac{\partial}{\partial x_k}(\rho\overline{u'_\iota u'_\jmath u'_k} + \overline{p(\delta_{kj}u'_k + \delta_{\iota k}u'_\jmath)})}_{(D_{T,ij}\ Turbulent\ Diffusion)} + \underbrace{\frac{\partial}{\partial x_k}\left(\mu\frac{\partial}{\partial x_k}\overline{u'_\iota u'_\jmath}\right)}_{(D_{L,ij}\ Molecular\ Diffusion)} - \underbrace{\rho\left(\overline{u'_\iota u'_k}\frac{\partial u_j}{\partial x_k} + \overline{u'_\jmath u'_k}\frac{\partial u_i}{\partial x_k}\right)}_{(P_{ij}\ Stress\ Production)} - \underbrace{\rho\beta(g_\iota\overline{u'_\iota\theta} + \overline{g_\iota u'_\jmath\theta})}_{(G_{ij}\ Buoyancy\ Production)} + \underbrace{\overline{P\left(\frac{\partial u'_\iota}{\partial x_\jmath} + \frac{\partial u'_\jmath}{\partial x_\iota}\right)}}_{(\emptyset_{ij}=Pressure\ Strain)} - \underbrace{\overline{2\mu\left(\frac{\partial u'_\iota}{\partial x_k}\frac{\partial u'_\jmath}{\partial x_k}\right)}}_{(\varepsilon_{ij}=Dissipation)} - \underbrace{2\rho\Omega_k(\overline{u'_\jmath u'_m}\varepsilon_{ikm} + \overline{u'_\iota u'_m}\varepsilon_{ikm})}_{(F_{ij}Production\ by\ system\ rotation)} + \underbrace{S_{user}}_{(User\ Defined\ Source\ term)} \quad (6)$$

From the above equation, C_{ij}, $D_{L,ij}$, P_{ij}, and F_{ij} do not need modeling. But, $D_{T,ij}$, G_{ij}, $\emptyset_{ij}$, and ε_{ij} must be modeled to attain closure [19].

2.2.2 Combustion model
Turbulent Flame Speed Closure Model (TFCM)

The hardest modeling challenge depends on the ability to have the appropriate closure for the averaged or filtered transport equations. An effective closure model is assumed to suit Navier-Stokes equations, the further step is to adopt a proper closure model for the transport equations accounting for the thermochemistry. Turbulent Flame Speed Closure Model (TFCM) basically relies on replacing the reactive scalar (Yi) by a dimensionless variable representing the reaction progress (c). The limits of progress variable broadened from c = 0 in the fresh reactants to c =1 in the fully burned products. The progress variable c is expressed as a mass fraction of one or more product species Y_P:

$$C = \frac{Y_p}{Y_{p\infty}} \quad (7)$$

where $Y_{P\infty}$ is the value of Y_P in complete adiabatic combustion.

The transport equation of progress variable is formulated here as:

$$\frac{\partial}{\partial t}(\rho C) + \frac{\partial}{\partial x_k}(\rho u_k C) = w + \frac{\partial}{\partial x_k}\left(\rho D_c \frac{\partial C}{\partial x_k}\right) \quad (8)$$

w represents the chemical reaction rate of c and ρD_c indicates the molecular diffusivity of c.
For RANS, the average transport equation of progress variable becomes;

$$\frac{\partial}{\partial t}(\bar{\rho}\tilde{C}) + \frac{\partial}{\partial x_k}(\bar{\rho}\,\widetilde{u_k}\tilde{C}) = \bar{w} + \frac{\partial}{\partial x_k}\left(\overline{\rho D_c \frac{\partial C}{\partial x_k}}\right) - \frac{\partial}{\partial x_k}\rho\overline{u_k'' C''} \quad (9)$$

The three terms stated in the right side of equation (9) need to be modeled as they are unclosed. The molecular transport, the second term in the right-hand side of equation (9) can be often ignored for high Reynold's number flows, while the closure modelling of the remaining terms will be presented in the upcoming paragraphs.

The closure of Reynold's flux term $\overline{\rho u''_k c''}$ is based on flamelet theory of Reynold's flux [4] which postulates that turbulent transport term (Reynold's flux) is balanced between mixing effect which driven by turbulence and acceleration resulted from heat liberated effect. Both effects work against each other, since turbulent mixing effect supports gradient transport while heat release effect supports counter-gradient transport. The model of turbulent transport term can be expresses as [20]:

$$\rho\overline{u_k'' C''} = \bar{\rho}\,\tilde{C}\,(1-\tilde{C})(\,\tau S_L - 2\alpha\, u') \quad (10)$$

Zimont developed simple closure model for the reaction rate term $\bar{w}$ of progress variable transport equation. This model was proposed on the basis of increasing flame brush thickness based on turbulent diffusion law, and spreads with an invariant combustion velocity. The reaction rate term $\bar{w}$ is stated as follow [21]:

$$\bar{w} = -\rho_u S_t \left|\frac{\partial C}{\partial x_i}\right| \quad (11)$$

where ρ_u and S_t unburnt density and turbulent flame speed respectively. The turbulent flame speed St can be modeled according to the following equation:

$$S_t = A u_t'^{3/4} S_l^{1/2} \alpha^{-1/4} l_t^{1/4} \quad (12)$$

where α, S_l, l_t and u'_t are thermal diffusivity of air-fuel mixture, laminar flame velocity, turbulent length scale and the root mean square of velocity respectively. A is a model constant varied according to fuel type. Finally, the turbulent flame closure model (TFCM) was examined against experimental data for various combustion applications [6,7]. In this work S_l for different fuel gas mixtures is obtained from [14].

Table 1 Inlet Fuel of the basic case

Fuel	W (W)	PCI (MJ/kg)	M (kg/kmol)	%V in mix	%m in mix	mdot(kg/s)	Vdot (l/min)	mdot (kg/(m^2*s))
H_2	823.4452	119.95	2.02	50	10.60312	6.86E-06	5.019652	0.008026
NH_3	1076.555	18.6	17.03	50	89.39688	5.78E-05	5.019652	0.067671
Total	1900					6.4E-05	10.39304	0.075697

2.3 Boundary Conditions

The burner output rating is kept constant at 1900 W for the three studied cases which are all of stoichiometric mixture of fuel and air. Table (1) presents the fuel condition for the case of ammonia/hydrogen of molar ratio of 1:1. Mass flow inlet boundary condition is selected at the combustor inlet while pressure outlet boundary condition is specified at combustor exit. Mixed thermal condition is specified to account radiation and convective losses. Convergence criteria is specified to be 10^{-6}.

3. RESULTS AND DISCUSSION

Various computational schemes have been adopted to investigate the interaction between flow field dynamics and combustion characteristics that would be affecting the stability of NH3/ H2 /Air flame at stoichiometric mixture emerging from an innovative design of swirl-bluff body stabilized burner with two different bluff body geometries. To obtain the optimal

grid for solving the present case study, a grid independency test was done as shown in figure 3. Quantification of the error for the axial velocity is presented from different mesh resolutions at 60000, 106000 and 150000 cells. It can be depicted that using 106000 cells saves the computational cost without affecting the solution accuracy. Cold flow case has been initially performed using Mixing Species Transport scheme to verify the model validity in simulating the flow field and mass transport of reacting species in a simple case with no reaction involved. Figure 4 displays the velocity contours inside the chamber including the premixing tube, where the present flow field is strongly affected by the bluff body configuration, the ratio between tangential and axial velocity components and Reynold's number. One of the main purposes of such burner design is to introduce air from tangential ports to create central recirculating motion that is intensified with the existence of a bluff-body at the core of the burner tip. The generated vortices and the localized recirculated flow developed from swirling motion played a major role to obtain a high degree of uniformity index (~96%) between air and H2/NH3 fuel at burner tip that assists in flame stabilization. Figure 5 presents a comparison between the flow field developed from the two burner designs (a) and (b). Both designs produce

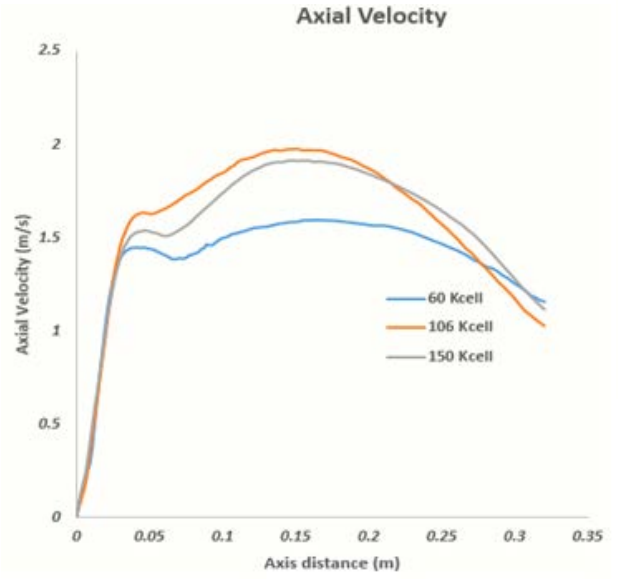

Fig. 3 Grid independency test through comparison of the axial velocity distribution for three different mesh sizes, 60000, 106000 and 150000 cells.

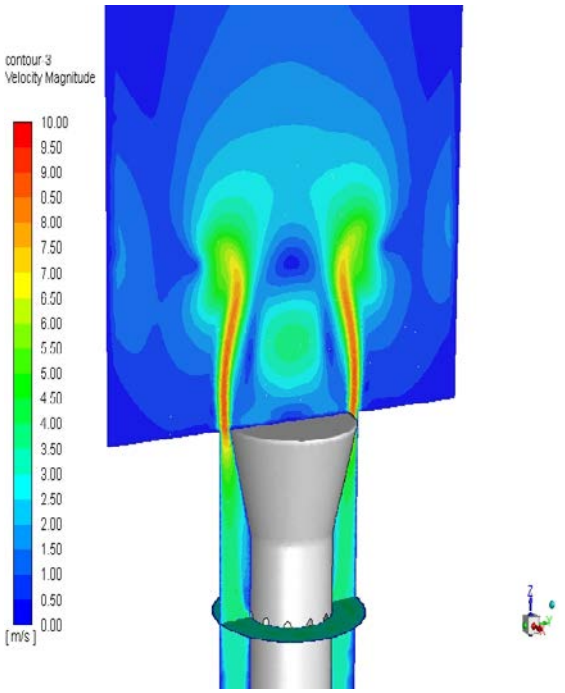

Fig.4: Axial velocity contours of cold flow stoichiometric mixture of 50%H_2/50%NH_3/air

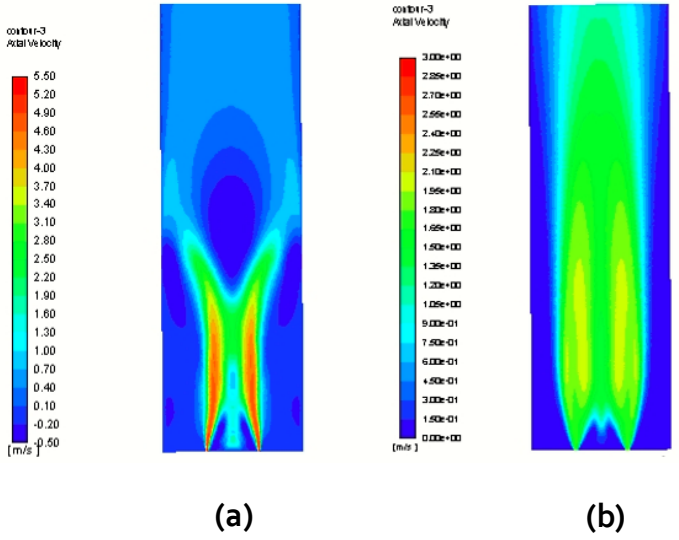

Fig.5: Comparison between axial velocity contours of burners (a) and (b) for cold flow stoichiometric mixture of 50%H_2/50%NH_3/air using 3D simulation Mixing species transport model

Symmetrical flow pattern around the central axis. Flow field developed from burner (a) is characterized by distinctive center recirculation zone established from the air swirling motion in addition to the

existence of bluff-body, an annular high velocity zone and an outer recirculation zone between the high velocity zone and the bounding walls. The flow pattern of burner (b) is attributed by streamlined jet flow shape. Flow field developed from burner (a) has superior characteristics in accelerating reaction rates and enhancing turbulence degree than developed from burner (b). Thus, it was decided to concentrate the rest of the analysis on the configuration of burner (a).

Activating reactive flow case by adopting axi-symmetric/Premixed Combustion scheme to investigate combustion characteristics for variant H2 addition in NH3 fuel is considered in this section. Figure 6 illustrates the contours of product formation rate at different fuel compositions (100% NH3, 75% NH3 and 50% NH3). Product formation rate is a normalized average of the overall reaction rate (sec-1), and it is also a valuable representative of the flame shape appearance. It can be depicted from figure 5 that adding 50% H2 to ammonia increases the overall burning rate (product formation rate) by 10 times when compared to 100% ammonia case. Pure ammonia combustion case is characterized by an elongated region of reaction zone (very long flame) and by adding more hydrogen, the flame (reaction zone) becomes shortened due to its high reactivity. The progress variable which is another chemical reaction indicator by having the potential to track the overall reaction zone of the local mixture is presented in figure 7 at various H2 concentration in H2/NH3 mixture. Adding more Hydrogen accelerates the reaction rate driving the involving mixture to rapidly react once it emerged from the premixing tube. Figure 8 displays the temperature contours for different fuel composition, where the largest extent of higher temperature regions is depicted for 50% of H2 enrichment case. For pure ammonia combustion case, a distinctive attribute of forming two wings of stratified temperature layers enclosed by the highest temperature layer of the burnt gases at the outer envelope and the lowest temperature of the unburnt mixture at the wing core is observed. This noticeable stratification of temperature is justified due to the slow reactivity of pure ammonia combustion. The axial velocity contours in figure 9 show that adding more H2 increases the burning rate leading to the rapid conversion of the unburnt mixture to burnt gases which develops lower velocity gradient throughout the chamber domain. However, a noticeable velocity gradient appears which can be explained as a result of slower density conversion rate form unburnt to burnt gases arising from slower reactivity of ammonia.

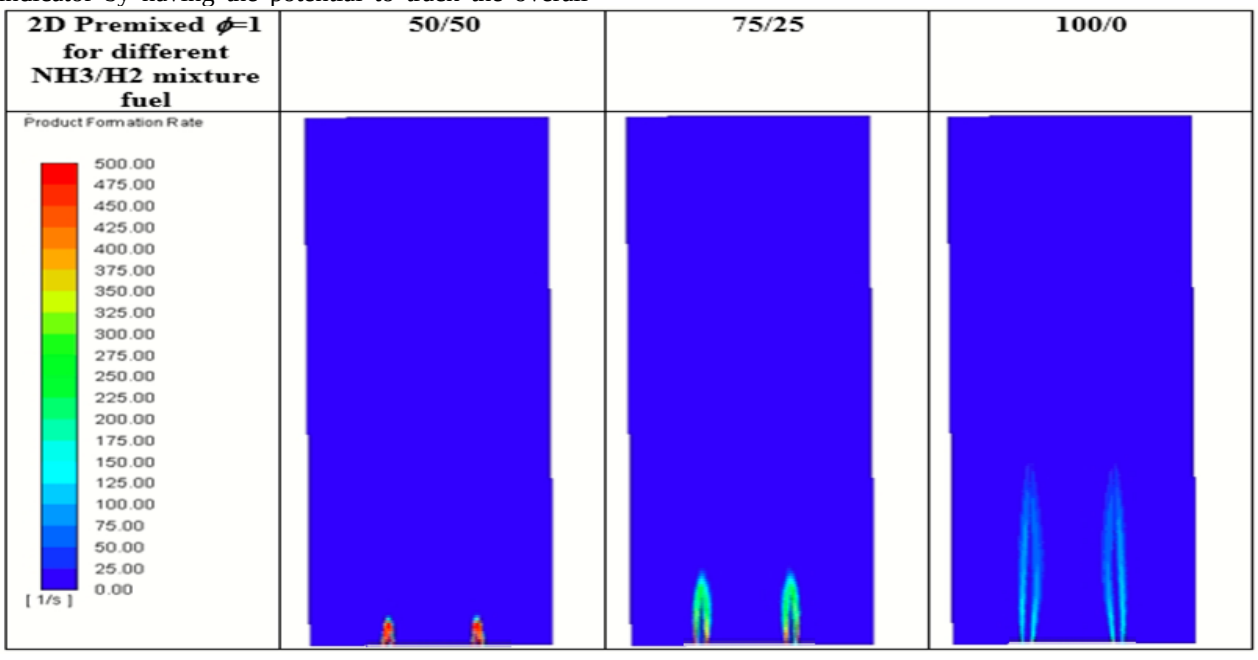

Fig.6: Comparison between product formation rate (s^{-1}) at different H_2 mixture fraction (50%, 25% and 0%) using axi-symmetric Simulation Premixed Combustion Model

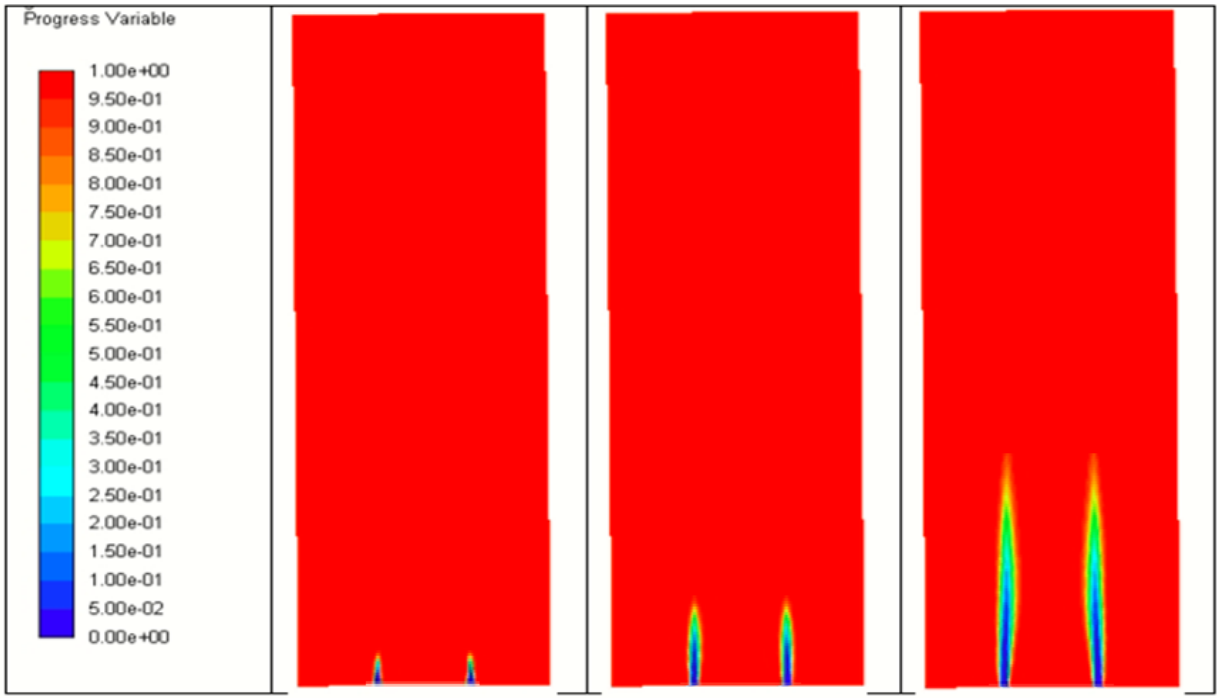

Fig.7: Comparison between product progress variable at H_2 fraction (50%, 25% and 0%/) using Premixed Combustion Model

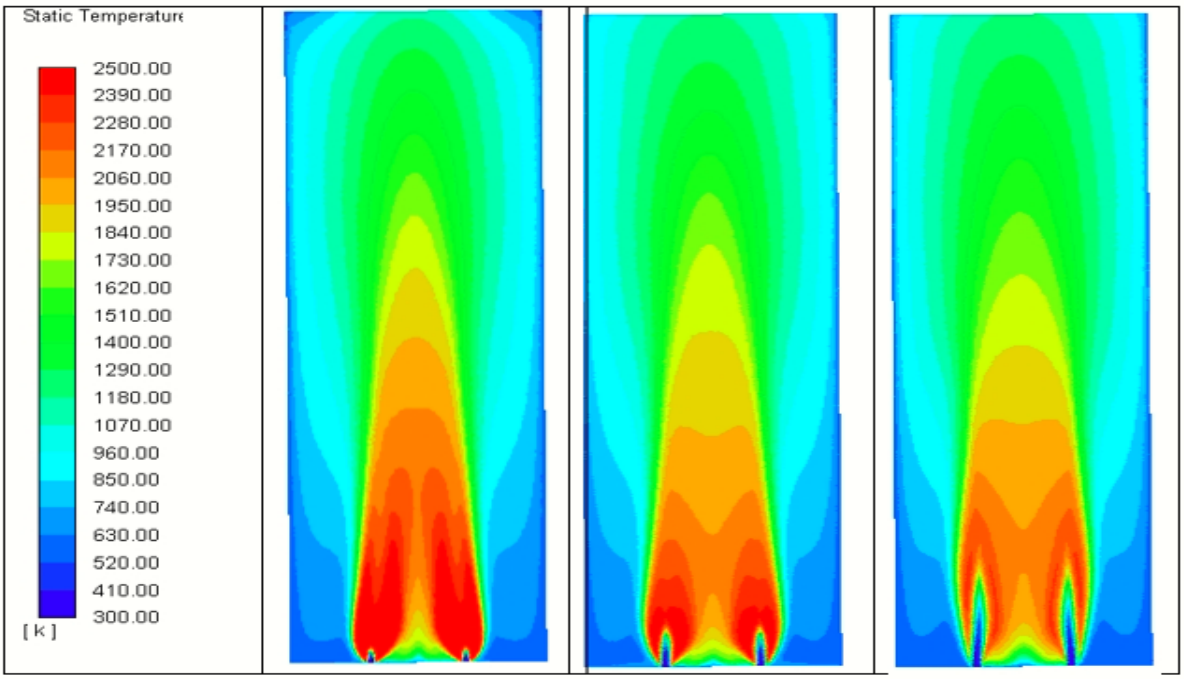

Fig.8: Comparison between temperatures at different H_2 mixture fraction (50%, 25% and 0%/) using Premixed Combustion Model

A more realistic case of issuing the air-fuel mixture at non-fully premixed case (uniformity index ~ 96) adopting partially-premixed model is considered to investigate the flame structure of H_2/NH_3/AIR mixture. Temperature contours presented in figure 10 shows that, adding more hydrogen, increases the mixture reactivity and flame speed as well. With higher increasing the flame speed, the flame approaches backward toward the premixing tube and flash-back phenomenon could take place at certain amount of H_2.

Radical concentration of OH is a good representative for tracking the reaction zone (flame sheet profile) where its contour is displayed at different amount of H_2 enrichment in figure 11. The higher reactivity of hydrogen for 50% H_2 50% ammonia case, obtains higher concentration of OH radical, at which the flame moves backward with higher enriching of H_2, leading to flash-black at certain value. Figures 12 and 13 confirm the same finding that has been mentioned earlier, adding more hydrogen to H_2/NH_3 mixture increases the reactivity of ammonia and consequently increases its turbulent flame speed and H_2O product. Further increasing of H_2 leads to rapidly move the flame front towards the premixing tube and there is threshold value at which flash-back takes place.

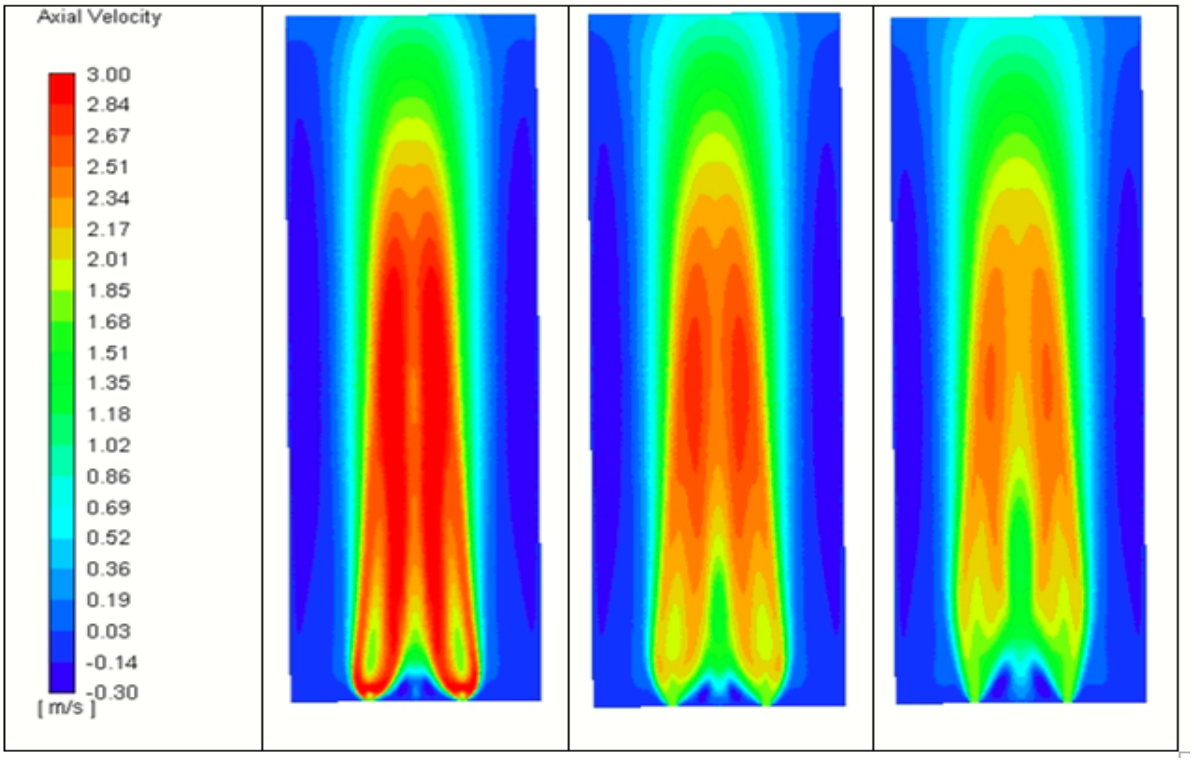

Fig.9: Comparison between axial velocities at different H_2 mixture fraction (50%, 25% and 0%/) using Premixed Combustion Model

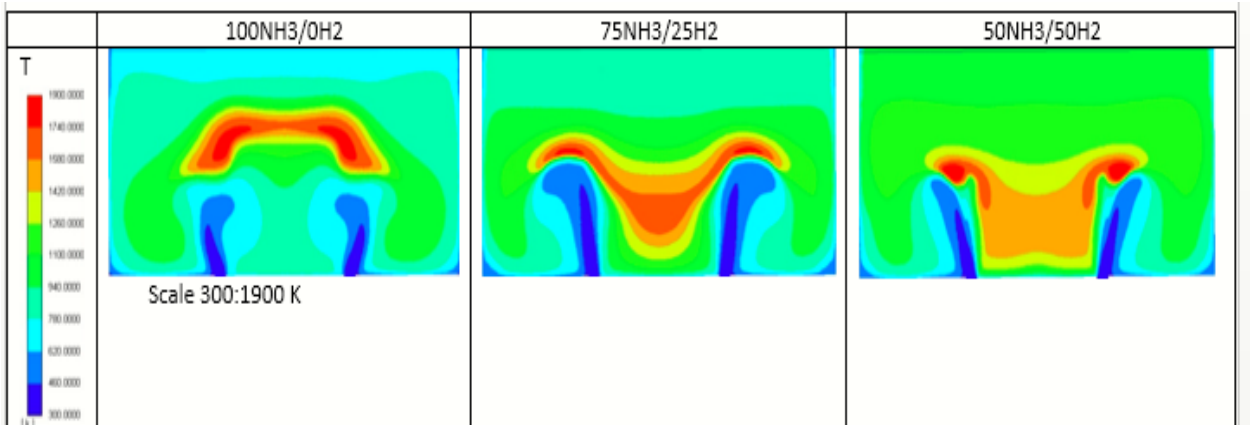

Fig.10: Comparison between temperatures at different H_2/NH_3 compositions (50%/50%, 25%/75% and 0%/100%) in burner (a) using Partially Premixed Combustion Model

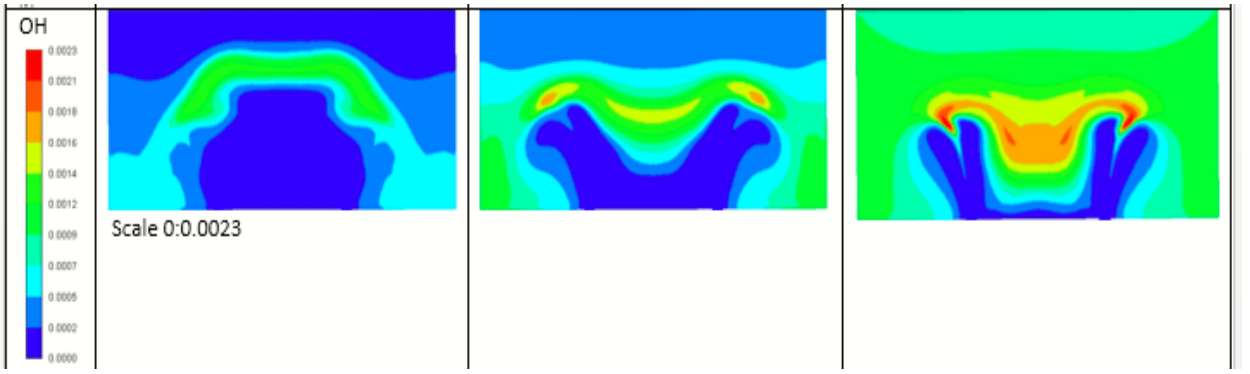

Fig.11: Comparison between OH concentration at different H_2/NH_3 compositions (50%/50%, 25%/75% and 0%/100%) in burner (a) using Partially Premixed Combustion Model

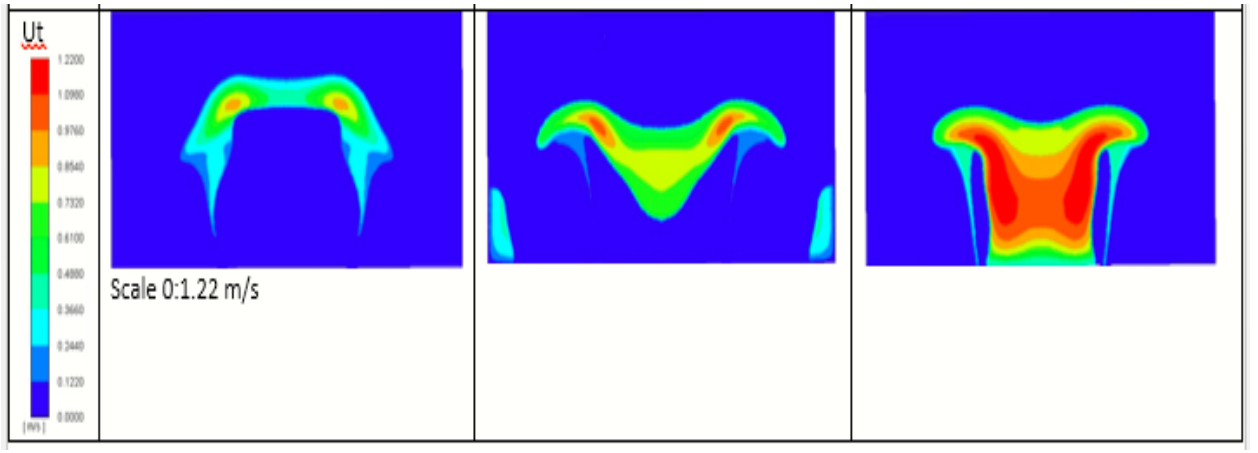

Fig.12: Comparison between the turbulent flame speeds at different H_2/NH_3 compositions (50%/50%, 25%/75% and 0%/100%) in burner (a) using Partially Premixed Combustion Model

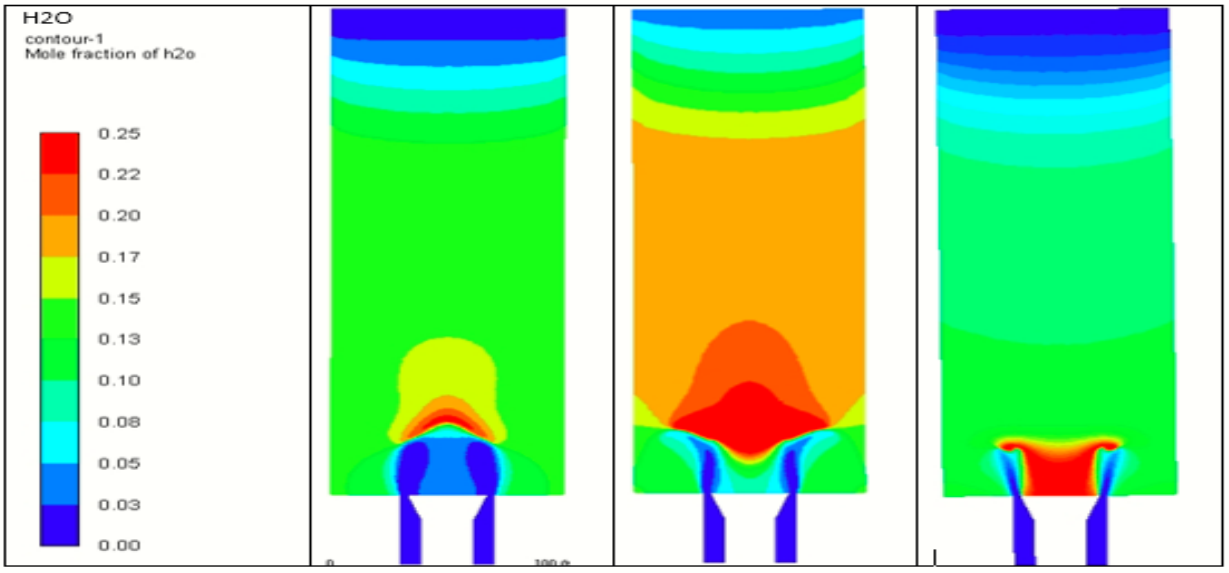

Fig.13: Comparison between H2O concentrations at different H_2/NH_3compositions (50%/50%, 25%/75% and 0%/100%) in burner (a) using Partially Premixed Combustion Model

4. CONCLUDING REMARKS

A numerical study was performed to assess the main combustion characteristics of stoichiometric mixtures of ammonia and hydrogen ammonia blended fuels in a swirled air and bluff body laboratory scale combustor. The cold flow analysis indicated that the tube prior to the burner achieves a mixing of around 95% allowing for treating the reacting downstream flow as either premixed or partially premixed. The flow aerodynamic pattern produced a central and outer recirculation zones surrounding a high velocity flow between the two for one of the two studied burners resulting in omitting the other one from further investigations. The study showed a longer flame length for the pure ammonia case due to its slow reactivity and slow laminar burning velocities. Increasing the mixture fraction of blended hydrogen 25 and 50 % resulted in decreasing the flame length and a ten-fold formation and reaction rates were observed amongst the numerical results. Some evidence that flash back takes place for the case of 50% hydrogen. Future work will incorporate detailed chemistry to study the NOx emissions for different ammonia hydrogen flames.

5. NOMENCLATURE

English

A model constant of Zimont
C reaction progress variable
$C_{i,j}$ convective term
D mass diffusivity
$D_{l.ij}$ molecular diffusion term
$D_{T,ij}$ Turbulent diffusion term
E total energy
E_a activation energy
F body force
g segregation factor
G_{ij} buoyancy production term
h enthalpy
J diffusion flux
k turbulent kinetic energy
Le Lewis number
l_t integral turbulent length scale
Ma Mach number
P_{ij} stress production
Pr Prandtl number
q_c combustion heat release
$\bar{q}$ Reynolds-averaged value of a general quantity q
$\tilde{q}$ Favre averaged value of a general quantity q
q" Reynolds-averaged value of a general quantity q
R universal gas constant
Re Reynolds number
S_L laminar flame speed
S_{Yk} source term of the k_{th} species
t time

t_{chem} Chemical time scale
T Temperature
T_{ad} Adiabatic flame temperature
u_i i^{th} component velocity
u' root mean square fluctuation velocity
w chemical reaction rate
x_i i^{th} Cartesian co-ordinate
Y_k mass fraction of the k_{th} species

Greek

α thermal diffusivity
χ ratio of specific heats
ε dissipation rate of turbulent kinetic energy
$\emptyset_{ij}$ pressure strain term
γ Kolmogorov length scale
λ_{eff} effective conductivity
μ_0 kinematic viscosity of unburned gas
ρ density
σ heat release parameter
τ_{ij} viscous stress tensor
σ heat release parameter
τ_{ij} viscous stress tensor

Acronyms

DNS Direct Numerical Simulation
LES Large-Eddy Simulation
RANS Reynolds-Averaged Navier–Stokes
TFCM Turbulent Flame Closure Model

6. REFERENCES

[1] L.M. Miller, D.W. Keith, Observation-based solar and wind power capacity factors and power densities, Environmental Research Letters. 13 (2018). https://doi.org/10.1088/1748-9326/aae102.

[2] A. Valera-Medina, H. Xiao, M. Owen-Jones, W.I.F. David, P.J. Bowen, Ammonia for power, Progress in Energy and Combustion Science. 69 (2018) 63–102. https://doi.org/10.1016/j.pecs.2018.07.001.

[3] H. Kobayashi, A. Hayakawa, K.D.K.A. Somarathne, E.C. Okafor, Science and technology of ammonia combustion, Proceedings of the Combustion Institute. 37 (2019) 109–133. https://doi.org/10.1016/j.proci.2018.09.029.

[4] W. JW. Erisman, MA Sutton, MA Galloway, J. Kilmont, Z, Winiwater, How a century of ammonia synthesis changed the world., Nat Geosci. 1 (2008) 636–639.

[5] N.A. Hussein, A. Valera-Medina, A.S. Alsaegh, Ammonia- hydrogen combustion in a swirl burner with reduction of NOx emissions, Energy Procedia. 158 (2019) 2305–2310. https://doi.org/10.1016/j.egypro.2019.01.265.

[6] A. Yapicioglu, I. Dincer, Performance assesment of hydrogen and ammonia combustion with various fuels for power generators, International Journal of Hydrogen Energy. 43 (2018) 21037–21048. https://doi.org/10.1016/j.ijhydene.2018.08.198.

[7] P.F. Henshaw, T. D'Andrea, K.R.C. Mann, D.S.K. Ting, Premixed ammonia-methane-air combustion, Combustion Science and Technology. 177 (2005) 2151–2170. https://doi.org/10.1080/00102200500240695.

[8] A. Hayakawa, Y. Arakawa, R. Mimoto, K.D.K.A. Somarathne, T. Kudo, H. Kobayashi, Experimental investigation of stabilization and emission characteristics of ammonia/air premixed flames in a swirl combustor, International Journal of Hydrogen Energy. 42 (2017) 14010–14018. https://doi.org/10.1016/j.ijhydene.2017.01.046.

[9] J. Li, H. Huang, N. Kobayashi, Z. He, Y. Osaka, T. Zeng, Numerical study on effect of oxygen content in combustion air on ammonia combustion, Energy. 93 (2015) 2053–2068. https://doi.org/10.1016/j.energy.2015.10.060.

[10] J. Konnov, A. A. and De Ruyck, Kinetic modelling of the thermal decomposition of ammonia, Combustion Science and Technology. 152 (2000) 23–37.

[11] J. Konnov, A. A. and De Ruyeck, No Title, Combustion Science and Technology. 168 (2001) 1–46.

[12] J. Konnov, A. A. and De Ruyeck, No Title, Combustion and Flame. 124 (2001) 106–126.

[13] C. Duynslaegher, F. Contino, J. Vandooren, H. Jeanmart, Modeling of ammonia combustion at low pressure, Combustion and Flame. 159 (2012) 2799–2805. https://doi.org/10.1016/j.combustflame.2012.06.003.

[14] X. Han, Z. Wang, M. Costa, Z. Sun, Y. He, K. Cen, Experimental and kinetic modeling study of laminar burning velocities of NH 3 /air, NH 3 /H 2 /air, NH 3 /CO/air and NH 3 /CH 4 /air premixed flames, Combustion and Flame. 206 (2019) 214–226. https://doi.org/10.1016/j.combustflame.2019.05.003.

[15] M.C. and M.Y. M. Franco, F. Ramos, R. Rocha, Development of a laboratory combustor for ammonia firing, in: 14th International Conference on Energy for a Clean Environment., Madeira, Portugal, n.d.

[16] FLUENT, A Theorey Guide, Canonsburg P. A. ANSYS Inc. (2016).

[17] W. Versteeg, H. K. and Malalasekera, An Introduction to Computational Fluid Dynamics The Finite Volume Method, Second Edi, Pearson, Prentice Hall, 2007.

[18] W. Launder, B. E., Reece, G. J. and Rodi, Progress in the Development of a Reynolds-Stress Turbulent Closure, Journal of Fluid Mechanics. 38 (1975) 537–566.

[19] Ansys Fluent 12.0 user's guide, "chapter 10 modeling

turbulence”, http://www.afs.enea.it/project/neptunius/docs/fluent/html/ug/node405.htm, (n.d.).

[20] T. Venynante, D., Trouve, A., Bray, K. N. C., and Mantel, Gradient and counter-gradient turbulent scalar transport in turbulent premixed flames, J. Fluid Mech. 332 (1997) 263–293. https://doi.org/https://doi.org/10.1017/S0022112096004065.

[21] V. Zimont, Gas premixed combustion at high turbulence, Turbulence Flame Closure Model, Experimental Thermal and Fluid Science. 21 (2000) 179–186.